available at www.sciencedirect.com

ScienceDirect

journal homepage: www.ejconline.com

Cell cycle and apoptotic effects of SAHA are regulated by the cellular microenvironment in HCT116 multicellular tumour spheroids

Valérie Lobjois[a], *Céline Frongia*[a], *Suzanne Jozan*[b], *Isabelle Truchet*[a], *Annie Valette*[a,*]

[a]*LBCMCP-CNRS UMR 5088, Université de Toulouse, 118 Route de Narbonne, F-31062 Toulouse, France*
[b]*Laboratoire d'Histologie-Embryologie, Faculté de Medecine, 31062 Toulouse, France*

ARTICLE INFO

Article history:
Received 20 March 2009
Received in revised form 7 May 2009
Accepted 20 May 2009
Available online 22 June 2009

Keywords:
Spheroids
Tumour microenvironment
SAHA
Cell cycle
Cytotoxicity
3D imaging

ABSTRACT

Using multicellular tumour spheroids (MCTS) of HCT116 colon carcinoma cells, we analysed the effects of SAHA (suberoylanilide hydroxamic acid), a histone deacetylase inhibitor (HDACi). We found that, although SAHA-induced histone acetylation and ROS level upregulation occur throughout the spheroid, inhibition of cell cycle progression and induction of apoptosis are dependent on cell microenvironment. SAHA-induced growth inhibition of HCT116 MCTS results from the inhibition of cell cycle progression and induction of apoptosis. At a low concentration SAHA decreases Ki-67 and cyclin A positive cells and increases p21 positive cells in the outer layer while it induces a ROS-dependent apoptosis in the central zone of the spheroid. Coimmunostaining of p21 and apoptotic cells confirms that SAHA effects are different depending on the position of the cells within the spheroid. At a higher dose, SAHA induces mitotic defects and survivin downregulation in the outer layer of cells resulting in an additional cytotoxic effect in this part of the spheroid. Together these findings show that SAHA-induced cytostatic and cytotoxic effects occur in different cell populations, indicating that the cellular microenvironment is an important determinant in the regulation of the effects of SAHA treatment. Consequently, the MCTS model appears to be a valuable advanced tool for evaluating the effects of SAHA treatment in combination with other anticancer agents.

1. Introduction

Malignant progression, resulting from genetic changes of cancer cells, is influenced by tumour microenvironment. Cell–cell interactions (including malignant cellular interactions) are important modulators of the malignant cell phenotype. Indeed, the behaviour of a cancer cell in a tumour is controled by its interactions with its immediate neighbours and the extracellular matrix, and its microenvironment. It is well established that for many chemotherapeutic drugs a solid tumour environment results in an increased level of drug resistance, a phenomenon called the multicellular resistance.[1] Multicellular resistance emerges as soon as cancer cells have established contacts with their microenvironment, homologous cells, heterologous cells or extracellular matrix. It is now well established that monolayer cultures, in which these complex interactions are lost, do not represent the characteristics of 3-dimensional (3D) solid tumours. 3D spheroid culture systems are providing new insights in tumour biology and it is now widely accepted that multicellular tumour spheroids (MCTS) more accurately reproduce the tumour microenvironment.[2,3] While growing, spheroids display a

* *Corresponding author:* Tel.: +33 561 558 111; fax: +33 561 558 109.
E-mail address: valette@cict.fr (A. Valette).
0959-8049/$ - see front matter
doi:10.1016/j.ejca.2009.05.026

gradient of proliferating cells.[3] These proliferating cells are located in the outer cell layers and the quiescent cells are located more centrally. When the central cells become deprived of oxygen and glucose, cell death and necrosis occur. This cell heterogeneity is similar to that found in avascular microregions of tumours. These MCTS models have been recently used to investigate the long-term efficacy of antitumoural agents in quiescent tumour microregions[4], showing that MCTS models allow the investigation of drug response while taking cell heterogeneity into account.

Recently, epigenetic regulation of gene expression has been the subject of a growing interest and as a result of this, the histone deacetylase inhibitors (HDACis) in particular are emerging as a new class of anticancer agents.[5,6] Among the HDAC inhibitors, suberoylanilide hydroxamic acid (SAHA) has undergone evaluation in phase I and phase II clinical trials.[7,8] SAHA is the first of the new generation of HDAC inhibitors to be approved by the US FDA for treating patients with CTCL.[6,9] Moreover, recent studies have shown that HDACis have promising anticancer activity in solid tumour malignancies when given in combination with carboplatin and paclitaxel[11] or with a topo II inhibitor.[10] Multiple mechanisms by which SAHA induces anticancer effects have been identified to date. Indeed, SAHA has been shown to induce p21-mediated G1 arrest, mitotic defects and cell death in cancer cells cultured as a monolayer. SAHA induces apoptosis via activation of the intrinsic apoptotic pathway[11] associated with downregulation of the expression of anti-apoptotic proteins[12] and activation of BH3-only proapoptotic protein. Reactive oxygen species also play a role in cell-death pathways induced by SAHA: SAHA induces transcriptional activation of the ROS scavenger thioredoxin in non-transformed cells[13] and in transformed cells this response is defective resulting in an increase in ROS.

The factors which determine whether a cancer cell undergoes apoptosis or cell cycle arrest after exposure to HDAC inhibitors remain to be determined. Drug concentration appears to be a critical factor as most HDACis exhibit cytotoxicity at higher doses and induce a G1 arrest at lower doses. The balance between HDACi-induced growth arrest or cell death can also be determined by the ratio between pro- and anti-apoptotic proteins pre-existing in the cell. Indeed, overexpression of Bcl-2 inhibits HDACi-mediated apoptosis but has no effect on the cell cycle.[14] Furthermore, specific differences between cell cycle regulation and apoptosis with respect to dependency on individual HDAC isoenzymes have recently been shown.[15]

We investigated how the cellular effects of SAHA are regulated in a 3D culture context. The MCTS model allowed us to show that the effects of SAHA depend on its concentration and on the position of the cell within the spheroid, arguing that the microenvironment can alter the balance between SAHA-induced cell cycle arrest and apoptosis.

2. Materials and methods

2.1. Cell lines

Human colon cancer cell line HCT116 (ATCC) was cultured in DMEM supplemented with 10% foetal calf serum. HCT116 p53–/– and the parental HCT116 cell line from which it was derived (HCT116 p53+/+) were generous gifts from Dr. Bert Vogelstein. These HCT116 clones were grown in McCoy's medium supplemented with 10% foetal calf serum.

2.2. Multicellular tumour spheroid (MCTS) generation

We have adapted the hanging-drop method[16,17] to produce HCT116 spheroids of similar diameters and cell numbers. Twenty microlitres drops containing 500 cells were suspended on the lids of agar-coated 24-well plates containing 1 ml of culture media. After the 48 h time period required for cell aggregation the spheroids were transferred to the culture medium. By using this technique we obtained single spheroids in 90–95% of the wells and the variation of size between spheroids is less than 10%.

2.3. MCTS growth quantification

The size of each spheroid was determined by measuring two orthogonal diameters ($d1$ and $d2$) using an inverted microscope fitted with a calibrated eye piece reticule. Spheroid volume was determined according to the formula: $V = 4/3\pi r^3$ where $r = 1/2\sqrt{d1 \times d2}$.

2.4. Immunohistochemistry on paraffin sections

Spheroids were rinsed with PBS and fixed in 4% neutral-buffered formalin (Sigma) for 3 h and then paraffin embedded. Sections were prepared as previously described.[17] Before incubation with the primary antibody, paraffin sections were subjected to antigen retrieval in 10 mM citrate buffer (pH 6.8) for 2×5 min. Sections were incubated for 1 h at room temperature with primary antibodies and were then rinsed. Revelation was then carried out using the streptavidin–biotin LSAB2+ kit (Dako) according to the manufacturer's instructions. The primary antibodies were used as follows: mouse monoclonal anti-p21 antibody (Oncogene Research Products, Cambridge MA; 1/100), anti-cyclin A (Abcam; 1/50), anti-Ki-67 (Dakocytomation; 1/50). Proportions of Ki-67 positives cells were determined by counting 1000 cells from 3 to 4 sections of differents spheroids.

2.5. Immunofluorescence on frozen sections

After fixation, spheroids were processed for 12 μm frozen sections. Sections were incubated with polyclonal anti-acetylated lysine (Stressgen, 1/200, 1 h at 37 °C) or the following combinations: mouse monoclonal anti-p21 (Calbiochem, 1/500, 1 h at 37 °C) and rabbit monoclonal anti-cleaved PARP1 (Epitomics, 1/1000, overnight at 4 °C) or anti-p21 and polyclonal anti-phosphorylated-histone H3 (Upstate, 1/1000, overnight at 4 °C). After washes in PBS/Triton 0.1% v/v, the secondary antibody was applied (Alexa 488-anti-mouse or Alexa 594-anti-rabbit, Molecular Probes, 1/800, for 1 h at room temperature). For double immunostaining, the first antibody was revealed and then sections were incubated with the second primary antibody and then revealed.

2.6. Two-photon laser microscopy analysis of SAHA-induced cytotoxicity

Spheroids treated as described above with 1 μM or 5 μM of SAHA were incubated in a propidium iodide solution (final concentration: 6 μg/ml) for 30 min before fixation in 4% neutral-buffered formalin (Sigma) for 2–3 h. Spheroids were then mounted in cover imaging chambers (Sigma) in Dako mounting media. Images were acquired with a confocal microscope SP5 (Leica) using a two-photon laser (820 nm). Images were analysed with the ImageJ software package by using the Leica Tiff Sequence plugin. Three to six spheroids were processed for each experimental condition. For each spheroid, the median intensity of the Z stack was calculated and the fluorescence intensity profiles were measured along five diameters. The five profiles were averaged for each spheroid and then for each experimental condition. Images were processed using ImageJ software and data analysis was performed by using Prism Software.

2.7. Measurement of intracellular reactive oxygen species (ROS) accumulation

We monitored intracellular ROS levels by using the2′7′-dichlorodihydrofluorescein diacetate acetyl ester (H_2DCF-DA, Invitrogen), which is non-fluorescent until the acetate groups are removed by cellular esterases and oxidation occurs within cells. H_2DCF-DA is membrane permeable and is oxidised rapidly to the highly fluorescent DCF in the presence of intracellular ROS.[18] After treatment, multicellular spheroids were incubated in medium containing 20 μM H_2DCF-DA in 135 mM NaCl, 5.4 mM KCl, 1.8 mM $CaCl_2$, 1 mM $MgCl_2$, 10 mM glucose and 10 mM HEPES for 1 h at 37 °C. Spheroids were then transferred into ice and immediately mounted in DAKO mounting media and were analysed by two-photon laser microscopy as previously described. ROS production was inhibited by incubating spheroids in the radical scavenger N-acetyl-L-cysteine (NAC) (10 mM)[19] for 48 h before fixation.

3. Results

3.1. Growth of HCT116 multicellular spheroids is inhibited by SAHA treatment

To study the effects of SAHA in the context of a 3D culture we developed a multicellular tumour spheroid (MCTS) model of the human HCT116 colon adenocarcinoma cell line (Fig. 1A and B). HCT116 MCTS reached 0.26 mm^3 (±0.03 SEM) after 8 days in culture, and the doubling time of their volume was 2 days. As shown in Fig. 1B, the addition of 5 μM SAHA prevented HCT116 MCTS growth as assayed by monitoring its inhibitory effect on the increase in spheroid volume.

A dose-dependent inhibition of HCT116 MCTS growth (Fig. 1C) was observed after 5 days of treatment with various concentrations of SAHA. Under these conditions the IC50 value of SAHA was 1.3 μM (±0.4 SEM). We compared the dose sensitivity of HCT116 p53–/– MCTS to SAHA treatment with that of the corresponding parental HCT116 p53+/+ MCTS. The observed IC50s were 0.8 (±0.2 SEM) and 0.5 μM (±0.1 SEM), respectively, showing that SAHA inhibited the growth of the spheroids prepared from these two isogenic cell lines with equivalent efficiencies.

To monitor the penetration of SAHA within the spheroids, we performed immunodetection of acetylated lysines on frozen sections. As shown in Fig. 1D, after SAHA addition we observed a global increase in lysine acetylation, suggesting that SAHA has penetrated the full thickness of the spheroids. This result showed that the MCTS model can be used to study SAHA effects in a 3D context.

3.2. Cell cycle effects of SAHA are induced in the outer layer of HCT116 MCTS

The internal structure of MCTS is dependent upon the establishment of nutrients and oxygen gradients which lead to a decreasing gradient of proliferation from the periphery to the centre of spheroid.[3] To characterise the proliferative changes occurring after SAHA addition, formalin-fixed paraffin-embedded HCT116 MCTS sections were first immunostained for the proliferation marker Ki-67. We found that in control HCT116 MCTS a large proportion of cells were positive for Ki-67 (59%), particularly those located on the outermost layers of the spheroids (Fig. 2A). A reduced percentage of Ki-67-positive cells was found in SAHA-treated MCTS (Fig. 2B and C). This effect of SAHA, detected at a low dose (1 μM) (44% of Ki-67 positive cells) (Fig. 2B), was increased after exposure of HCT116 MCTS to a higher dose of SAHA (5 μM) (17% of Ki-67 positive cells) (Fig. 2C). At this SAHA concentration, Ki-67 staining revealed that the remaining positive cells presented with giant nuclei (Fig. 2C). Immunodetection of phosphorylated-histone H3 (pH3) (Fig. 2G–I) revealed that after a 5 μM treatment, which completely inhibits MCTS growth, a sizeable number of mitotic cells was still present. The proportion of cyclin A positive cells, located in the proliferative layers at the periphery of the spheroid, decreased in SAHA-treated HCT116 MCTS, and here again a more significant effect was observed at a dose of 5 μM (Fig. 2D–F).

The cyclin-dependent kinase inhibitor p21, a direct target of SAHA, is upregulated which can lead to cell cycle arrest at the G1/S transition.[20] We observed that p21 was only detected in the nuclei of a few cells within the control HCT116 MCTS (22%) (Fig. 3A and D). Treatment with 1 μM SAHA increased the number of p21 positive cells (35%). This increase occurred in the proliferative layer, with these cells displaying both nuclear and cytoplasmic staining (Fig. 3B and E). The proportion of p21 positive cells was not significantly changed in the intermediate and the central zones (corresponding to the Ki-67 negative area) of the HCT116 MCTS. After a 5 μM SAHA treatment, this increase in the proportion of p21 positive cells in the outer layer of the HCT116 MCTS was no longer observed (22% of p21 positive cells) (Fig. 3C and F).

Survivin is a bifunctional protein able to regulate cycle progression in mitosis as a passenger protein and to block apoptic pathways as a member of the IAP protein family.[21] It has been recently shown that SAHA-induced mitotic defects can been mediated by a transcriptional modulation of PLK1 and survivin.[22] Using the MCTS model we observed that survivin is regionally expressed, indeed it was essentially located in the proliferative outer cell layers and the more central spheroid core (Fig. 3G and J). As shown in tumour biopsis[23] we

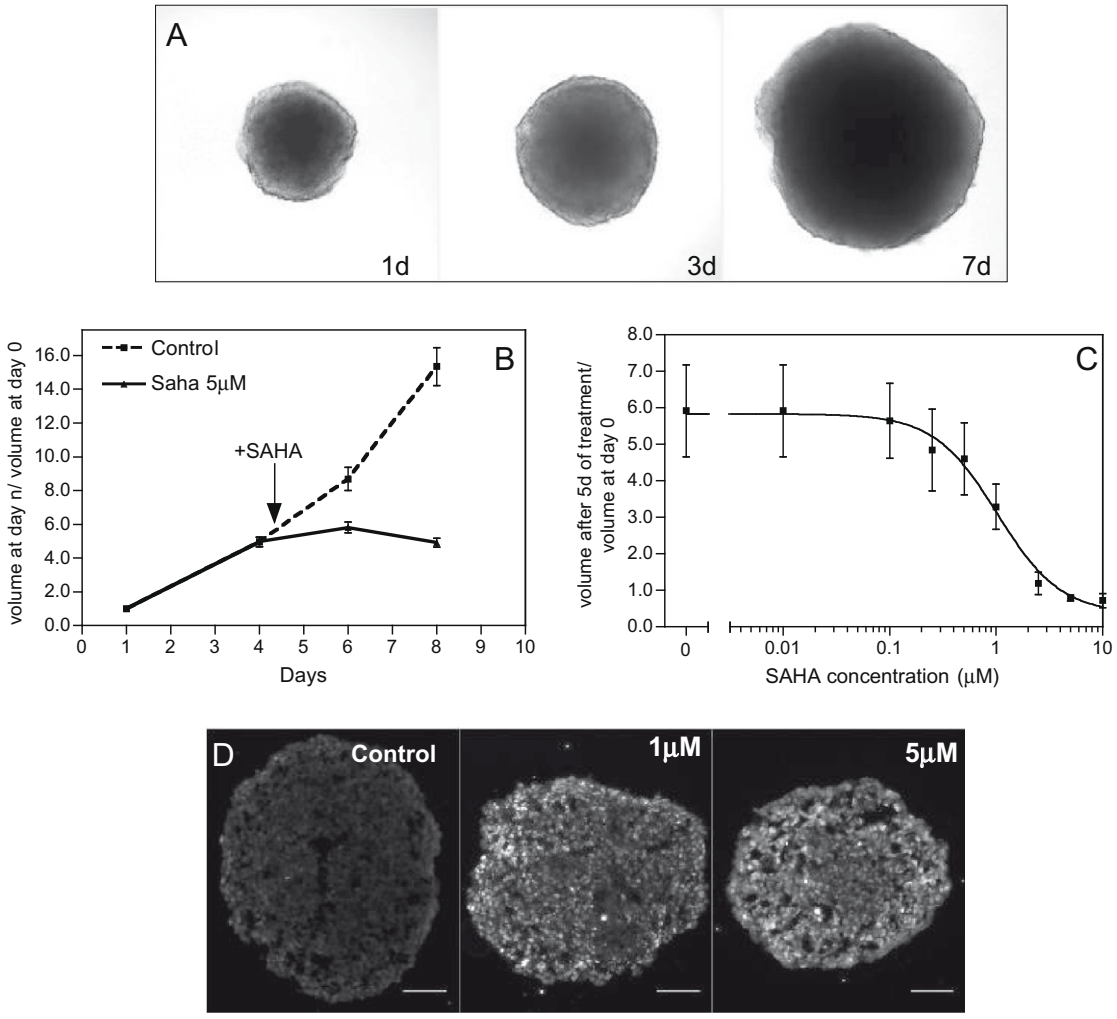

Fig. 1 – Effect of SAHA on HCT116 MCTS growth. (A) HCT116 MCTS visualised by phase contrast microscopy after 1, 3 and 7 days of culture. (B) Time-course of growth of HCT116 MCTS spheroid volume. The HCT116 MCTS were cultured in DMEM for 4 days and then SAHA was added or not. The volume of each spheroid was measured on the day of culture initiation and at the indicated days. The relative spheroid volume (ratio of the volume of the spheroids at day *n* to the volume of the spheroids on day 0) is plotted as a function of time. Results represent the mean ± SEM of four independent experiments; in each experiment four spheroids were measured. (C) SAHA dose-dependent effect. Spheroids were grown in DMEM for 5 days; indicated concentrations of SAHA were added for a 5-days additional period. The size of the spheroids was measured. The relative spheroid volume (ratio of the volume of the spheroids 5 days after SAHA treatment to the volume of the spheroids at the time of SAHA addition) is plotted as a function of SAHA concentration. Results represent the mean ± SEM of three experiments, in each experiment at least three spheroids were measured. (D) Immunodetection of acetylated lysines on frozen sections of control HCT116 MCTS or HCT116 MCTS treated with 1 μM or 5 μM of SAHA for 3 days. The scale bar corresponds to 100 μm.

found that survivin is detected both in the nucleus and in the cytoplasm of positive cells. Survivin expression is partially inhibited in the proliferating cells at 1 μM SAHA (Fig. 3H and K), and strongly downregulated at 5 μM SAHA (Fig. 3I and L) suggesting that survivin could participate in mitotic defects (Fig. 2I) observed at 5 μM in the outer cell layer of SAHA-treated HCT116 MCTS.

Taken together, these results show that in a 3D organisational context, SAHA exerts its cell cycle effects on the peripheral cell layers of the MCTS and that the nature of cell cycle effects varies depending on the SAHA concentration, i.e. at a low concentration a p21-mediated effect was observed while at a higher concentration, mitotic defects associated with survivin downregulation occur. This suggests that, depending on its concentration, SAHA activates different cell cycle checkpoints.

3.3. *The cytotoxic effect of SAHA is dependent on both its concentration and the position of the cells within the spheroids, and involves ROS production*

The therapeutic potential of SAHA also results from its ability to selectively induce apoptosis in tumour cells. To study

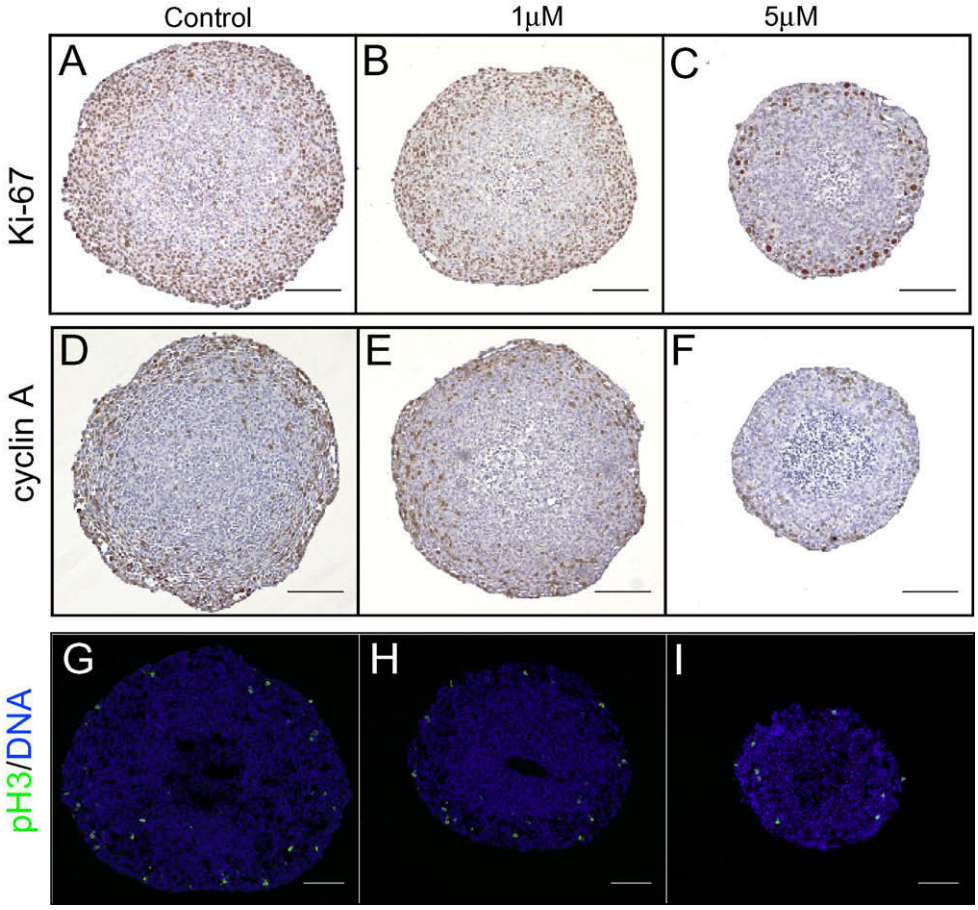

Fig. 2 – Cell cycle effect of SAHA in HCT116 MCTS. HCT116 MCTS were untreated (control) or treated with 1 μM or 5 μM SAHA for 3 days. Expression and distribution of Ki-67 (A–C) and cyclin A (D–F) were analysed by immunodetection on 6 μm paraffin sections. (G–I) Immunodetection of phosphorylated-histone H3 (pH3) and DNA staining by DAPI on 12 μm frozen sections. Images were collected using a X10 objective. The scale bar corresponds to 100 μm.

the apoptotic effect of SAHA treatment, SAHA-induced apoptosis in the HCT116 MCTS was examined using immunodetection of the cleaved form of PARP (Fig. 4A–C) on frozen sections. We found that compared to control HCT116 MCTS, a 1 μM SAHA treatment induced a significant increase in the proportion of apoptotic cells. Moreover, in contrast to our observations on SAHA-induced cell cycle effects, the cells which undergo apoptosis after a 1 μM SAHA treatment were not those of the peripheral cell layers, but those located within the deeper layers of HCT116 MCTS. Identical results were obtained using TUNEL staining (data not shown).

In order to further study this concentration-dependent regionalisation of SAHA-induced cytotoxicity, HCT116 MCTS that had been either left untreated, or treated with 1 μM or 5 μM SAHA were incubated in propidium iodide to stain dead cells. A 3D analysis was performed on whole-mounted spheroids using two-photon laser microscopy (Fig. 4D–F). Quantification of the fluorescence was performed on several spheroids for each experimental condition and the results are presented relative to the position of the centre of the spheroid in order to account for variations in spheroid diameter due to growth inhibition (Fig. 4G). After 3 days, a 1 μM SAHA treatment of HCT116 MCTS induced cytotoxicity in the intermediate and central layers but not in the outer proliferative cell layers (Fig. 4E and G). At a concentration of 5 μM, SAHA had a cytotoxic effect not only on the intermediate and central layer cells but also on the external proliferative cells (Fig. 4F and G). These results show that at a concentration of 1 μM, SAHA has a cytotoxic effect only on quiescent cells and that at a higher dose this effect is extended to proliferative cells.

It has been reported that SAHA induces the production of ROS in cancer cells cultured as monolayers.[24] Here, we found that HCT116 MCTS cultured with 1 μM SAHA for 24 h showed an important accumulation of ROS compared to control HCT116 MCTS (Fig. 5A and B). Results shown in Fig. 5B indicate that this ROS increase occurred throughout the spheroid. To determine the functional contribution of this increase in ROS levels in the induction of SAHA cytotoxic effects, HCT116 MCTS were treated with 1 μM SAHA in the presence or absence of the free radical scavenger N-acetyl-cysteine for 48 h. As shown in Fig. 5D, N-acetyl-cysteine (NAC) induced a decrease of SAHA-induced apoptosis in the centre of the spheroid. This result has been confirmed by a 3D analysis of

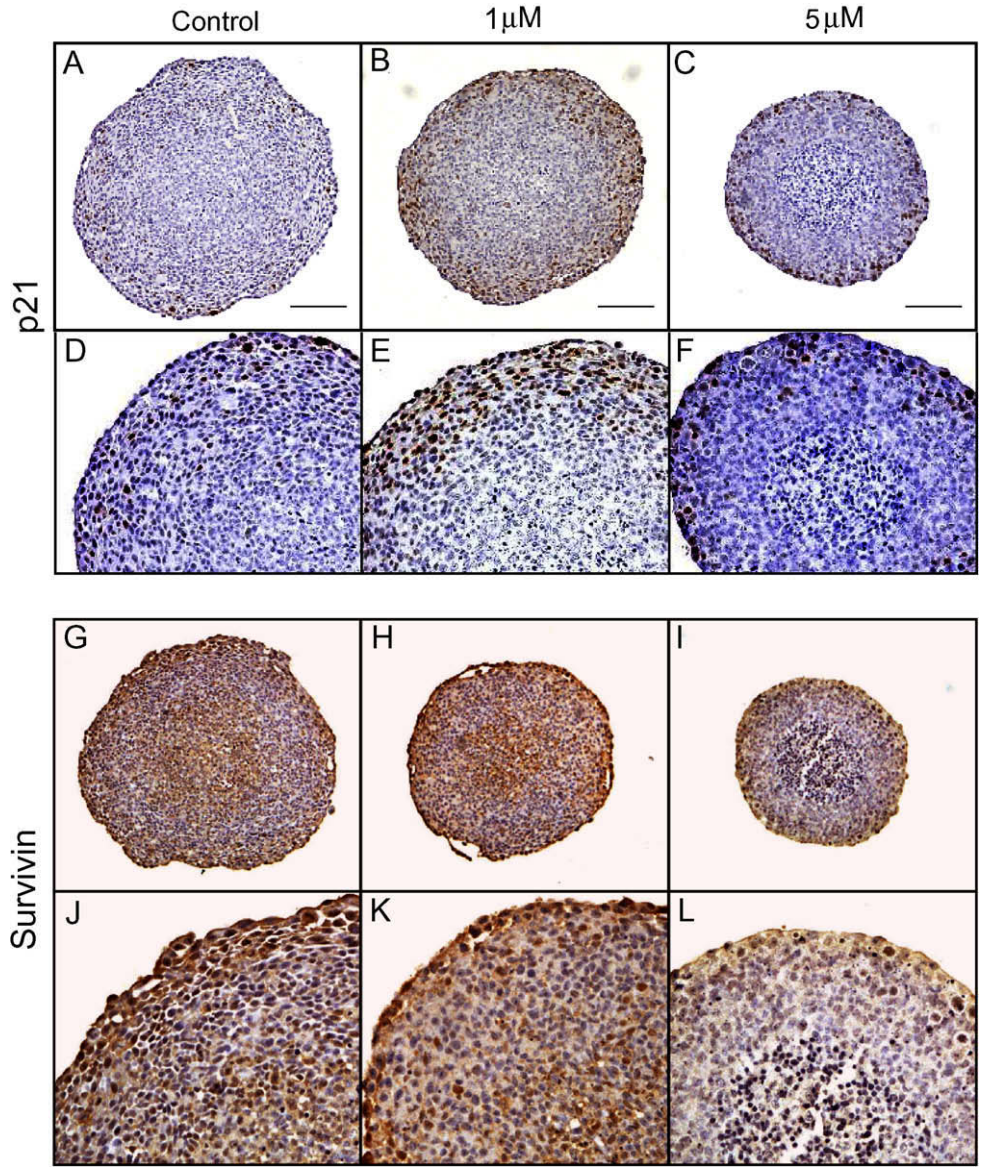

Fig. 3 – Regulation of p21 and survivin by SAHA. (A–F) Immunodetection of p21 on 6 μm paraffin sections. A–C were collected using a X5 objective. D–F correspond, respectively, to the same spheroids imaged using a X20 objective. (G–L) Immunodetection of survivin on 6 μm paraffin sections. G–I were collected using a X5 objective. J–L correspond, respectively, to the same spheroids imaged using a X20 objective.

the SAHA-induced cytotoxicity on entire spheroids using two-photon laser microscopy after propidium iodide incorporation (data not shown).

3.4. *The p21-mediated cell cycle effect and the cytotoxic effect of SAHA are dissociated in a microenvironment-dependent way*

To confirm that these SAHA-induced apoptotic and cell cycle effects occur in different cell populations, double-immunofluorescence staining of the cleaved form of PARP and p21 was performed on HCT116 MCTS treated with 1 μM SAHA (Fig. 6B). Under these experimental conditions, upregulation of p21 and induction of apoptosis occur in different cell population within the spheroid (Fig. 6B).

4. Discussion

The Multicellular tumour spheroid model mimics the *in vivo* situation more closely than two-dimensional culture systems. MCTS display a gradient of proliferation, with proliferative cells being located in the outer cell layers whereas quiescent cells are located more centrally. It has been previously shown that when the central cells become deprived of oxygen and glucose, cell death and necrosis occur.[3] Here, we found that cancer cells heterogeneity is involved in the response of HCT116 colon cancer cells to SAHA. Indeed, whereas SAHA induces an increase in both the level of acetylated lysine and ROS levels throughout the entire spheroid, the nature of the response of HCT116 cells depends on both SAHA concentrations and the position of cells within the

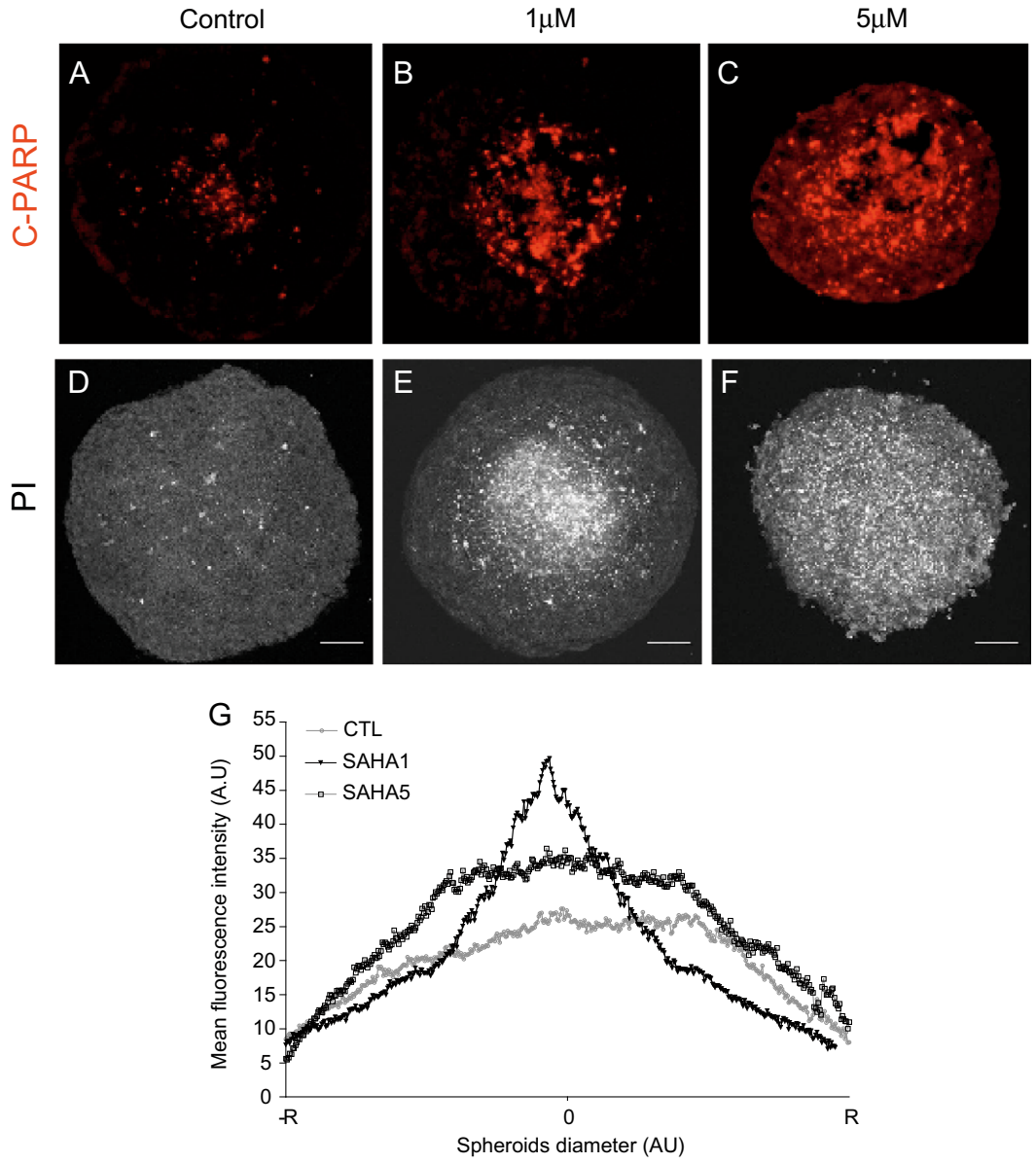

Fig. 4 – Apoptotic effect of SAHA on HCT116 MCTS. (A–C) Expression and distribution of the cleaved PARP (C-PARP) on control HCT116 MCTS (A) or MCTS treated for 3 days with 1 μM (B) or 5 μM SAHA (C). (D–G) 3D analysis of SAHA-induced cytotoxicity. Control HCT116 MCTS (D) or MCTS treated with 1 μM (E) or 5 μM (F) of SAHA were incubated with propidium iodide before fixation. Whole spheroids were imaged using two-photon laser microscopy. Maximal projections along Z-axis are shown. The mean of the median fluorescence intensity along five Feret's diameter per spheroids (3–6 spheroids per condition) is plotted (G). The X-axis represents the relative position to the centre of the spheroids and the fluorescence on the Y-axis is expressed in A.U. Mean standard error is ±0.4. R means radius.

spheroid. The cell cycle effect of SAHA occurs in the outer cell layers depending on SAHA concentration: a p21-associated cytostatic effect at a low dose and mitotic defects at a higher dose. The apoptotic effect occurs only in the centre of the spheroid at a low dose and affects all the layers at a higher dose. Indeed, apoptotic and cell cycle effects occur in the same cell population at high doses of SAHA but these two effects are dissociated by cell microenvironment at low doses. These results show that the use of a 3-dimensional culture allows the dissociation of SAHA cytostatic and cytotoxic effects. They agree well with a recent *in vivo* study in which R306465, a novel HDACi, induces *p21* gene activation in cell clusters, whereas histone H3 acetylation was observed throughout the tumour tissue[25] further supporting the idea that the spheroid model better reflects the *in vivo* behaviour of cancer cells.

SAHA induces a time- and dose-dependent inhibition of HCT116 MCTS growth. The growth of HCT116 MCTS

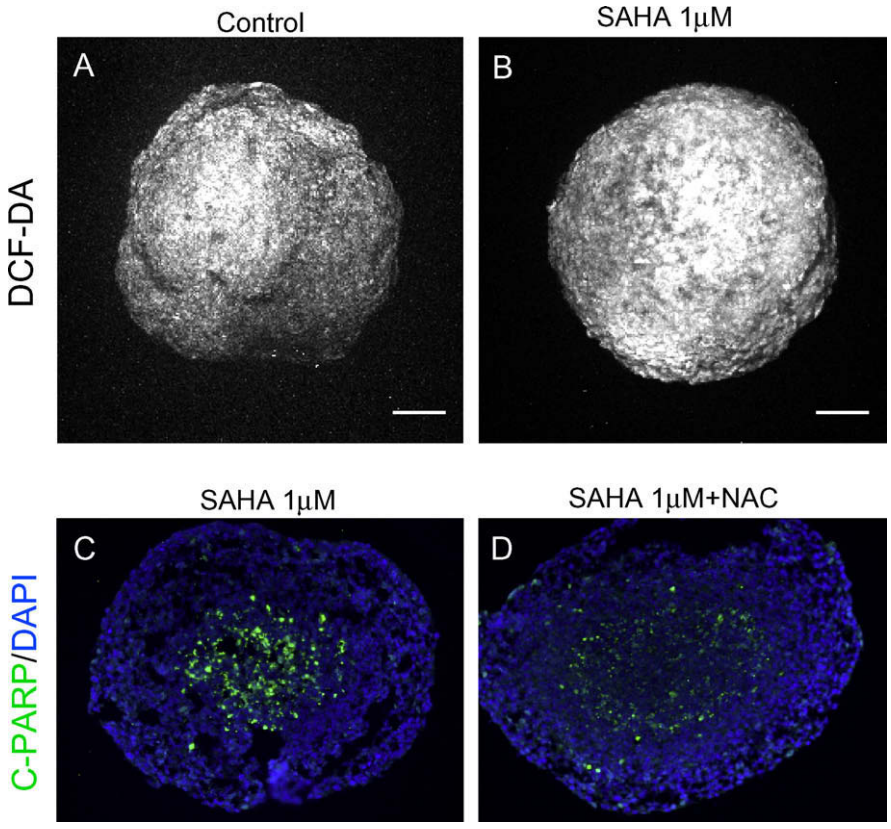

Fig. 5 – SAHA apoptotic effect involves ROS production. (A, B) ROS production monitored by using the fluorescent H2DCF-DA in control HCT116 MCTS (A) and 24 h after a 1 μM SAHA treatment (B). DCF fluorescence was analysed by two-photon laser microscopy on whole-mounted MCTS. Scale bar corresponds to 100 μm. (C, D) Immunodetection of the cleaved PARP (C-PARP) on frozen sections of HCT116 MCTS treated for 48 h with 1 μM of SAHA in the absence of (C) or in the presence of 10 mM of the free radical scavenger N-acetyl-L-cysteine (NAC) (D).

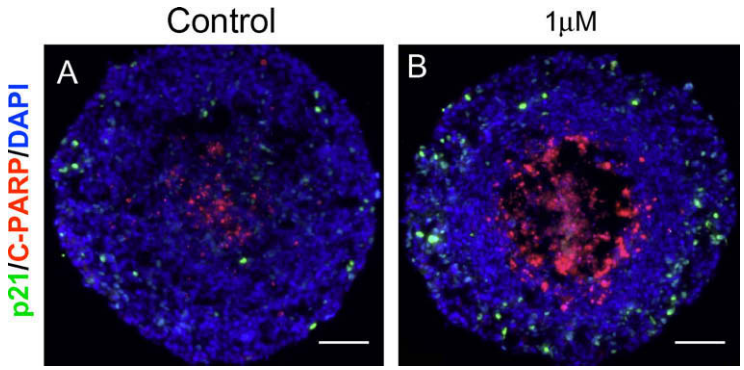

Fig. 6 – SAHA cell cycle and cytotoxic effects are dissociated in a microenvironment-dependent way. Co-immunodetection of p21 (green) and cleaved PARP (red) on control MCTS (A) and 1 μM SAHA-treated spheroids (B). DNA is stained using DAPI. Scale bar represents 100 μm.

generated from both p53-null cells and p53 wild-type cells was inhibited to an equivalent extent by SAHA treatment indicating that, as has been previously shown[26], the antiproliferative effect of SAHA on colon cancer cells is independent of p53 status. This SAHA-induced inhibition of HCT116 MCTS growth results from its ability to trigger both a cytostatic and a cytotoxic effect. The cytostatic effect is observed at a low dose of SAHA in the outer cell layers, it is associated with a downregulation of cyclin A expression and an upregulation of p21 leading to a decrease in the proportion of Ki-67 positive proliferative cells. The cytotoxic effect of SAHA is restricted to the central zone of the spheroid at a low dose and occurs in the entire spheroid at a high dose. Indeed, the analysis of the localisation of dead cells using two-photon laser microscopy and immunodetection of PARP cleavage clearly indicated that, at a low SAHA concentration, dead cells are only

detected in the non-proliferative cell population located within the central zone of the spheroid, whereas the cell death occurs thoughout the spheroid at a higher dose. In MCTS treated with a low dose of SAHA, our results of the coimmunostaining of p21 and the cleaved form of PARP clearly indicate that the SAHA-dependent cell cycle and apoptotic effects were induced in different cell populations within the spheroid further demonstrating that at this dose of SAHA these two SAHA effects are exclusive.

Whereas a p21-mediated cell cycle arrest is induced by low doses of SAHA, a mitotic checkpoint is activated at higher SAHA concentrations. Indeed, after SAHA treatment at a dose which completely blocks MCTS growth, the increase in the proportion of p21 positive cells was no longer observed and phosphohistone H3 positive mitotic cells were still detected, suggesting that SAHA, as has been previously shown[27], induces mitotic defects. Two observations further argue in favour of this hypothesis: (1) the presence of giant nuclei in the outer cell layers and (2) the accumulation of abnormal mitoses detected by DAPI staining (data not shown) in HCT116 MCTS treated with a 5 μM dose of SAHA. SAHA-induced mitotic defects are associated with the induction of apoptosis in the outer cell layer. It has been previously shown that mitotic defects result in cell death either by apoptosis or by mitotic catastrophe.[28] We also observed an important decrease in survivin expression in the outer cell layer of SAHA-treated MCTS. Survivin is a bifunctional protein able to regulate cell cycle progression in mitosis as a passenger protein and to block apoptic pathways as a member of the IAP protein family.[21] It has been recently shown that SAHA-induced mitotic defects can be mediated by a transcriptional modulation of PLK1 and survivin[22] in addition to transcription-independent defects resulting from an aberrant acetylation of histones in the pericentric heterochromatin.[29] Survivin has also been involved in SAHA-induced apoptosis. Taken together we hypothezise that, at a high SAHA concentration, survivin plays a role in both mitotic checkpoint activation and induction of apoptosis in the outer cell layer of HCT116 MCTS. The importance of SAHA concentrations in the determination of the nature of SAHA cell cycle and cytoxic effect has been previously shown in monolayer culture.[26,30] The use of a spheroid model allows us to show that the nature of the SAHA effect is regulated not only by SAHA concentration but also by the position of cells within the spheroid.

Thus, questions arise regarding the specificity of the apoptotic effect of SAHA on the non-proliferative central zone cell population, and the resistance of the proliferative outer layer cells to the cytotoxic effect of SAHA treatment. We hypothezise that mechanisms that facilitate apoptosis could exist in low-proliferating/hypoxic cells whereas mechanisms protecting cell from SAHA-induced apoptosis could take place in the proliferating cells. The fact that apoptosis takes place in the very slowly proliferating central cell population of the spheroid is in agreement with previous studies showing that HDACis are able to kill cancer cells arrested by serum starvation or expression of the cyclin-dependent kinase inhibitor $p16^{Ink4a}$.[31,32] The accepted range of oxygen diffusion is 150 to 300 μm, indicating that cells targeted with low doses of SAHA are hypoxic cells. Indeed, it has been shown using pimonidazole staining that hypoxia starts approximatively 150 μm from the surface of the spheroids and increases towards the centre.[33] We observed that SAHA triggers ROS production in the entire spheroid. However using the free radical scavenger NAC we showed that SAHA-induced ROS-dependent cytotoxic effect is only observed in the centre of the spheroid indicating that ROS are necessary but not sufficient to mediate the SAHA apoptotic effect. Taken together these observations suggest that another factor which is not present in the proliferating cells allow SAHA to trigger apoptosis. Concerning the molecular mechanisms that prevent the cells of the outer layers entering apoptosis after SAHA treatment, different studies have clearly shown that p21 expression inhibits cell death induced by HDACi treatment.[26,34] Different studies have clearly shown that p21 inhibits cell death induced by HDACi. The cells in which p21 expression increases after SAHA addition do not enter apoptosis, arguing in favour of an anti-apoptotic function of p21 leading to a regionalisation of this SAHA-induced apoptotic effect.

Overall the results of our study provide a description of SAHA effects in a cell context more relevant to the *in vivo* situation. The ability of SAHA to target different cell populations and in particular to trigger apoptosis in slowly proliferating cells make SAHA a promising antitumoural agent with potential therapeutic applications in human carcinoma. An ongoing challenge will be to identify combinations of compounds that will broaden the efficacy of SAHA. Since our results highlight the value of 3D studies for revealing the importance of the cellular microenvironment in the response of cancer cells to SAHA, combination studies in such a model will allow the targeting of cells with distinct proliferative status, as found in tumours.

Conflict of interest statement

None declared.

Acknowledgements

We acknowledge Didier Trouche, Bernard Ducommun, Sherilyn Goldstone and Andrew Russell for corrections and comments. We gratefully thank Viviane Blanco for technical assistance in the histochemical experiments. We also acknowledge the use of the imaging facilities of the CBD-IFR109. Valerie Lobjois is the recipient of a post-doctoral fellowship from la Ligue Nationale Contre le Cancer.

REFERENCES

1. Desoize B, Jardillier J. Multicellular resistance: a paradigm for clinical resistance? *Crit Rev Oncol Hematol* 2000;**36**(2–3):193–207.
2. Friedrich J, Ebner R, Kunz-Schughart LA. Experimental anti-tumour therapy in 3-D: spheroids–old hat or new challenge? *Int J Radiat Biol* 2007;**83**(11–12):849–71.
3. Sutherland RM. Cell and environment interactions in tumour microregions: the multicell spheroid model. *Science* 1988;**240**(4849):177–84.

4. Mellor HR, Ferguson DJ, Callaghan R. A model of quiescent tumour microregions for evaluating multicellular resistance to chemotherapeutic drugs. *Br J Cancer* 2005;**93**(3):302–9.
5. Marks PA, Richon VM, Breslow R, Rifkind RA. Histone deacetylase inhibitors as new cancer drugs. *Curr Opin Oncol* 2001;**13**(6):477–83.
6. Xu WS, Parmigiani RB, Marks PA. Histone deacetylase inhibitors: molecular mechanisms of action. *Oncogene* 2007;**26**(37):5541–52.
7. Marks PA. Discovery and development of SAHA as an anticancer agent. *Oncogene* 2007;**26**(9):1351–6.
8. Piekarz R, Bates S. A review of depsipeptide and other histone deacetylase inhibitors in clinical trials. *Curr Pharm Des* 2004;**10**(19):2289–98.
9. Duvic M, Talpur R, Ni X, et al. Phase 2 trial of oral vorinostat (suberoylanilide hydroxamic acid, SAHA) for refractory cutaneous T-cell lymphoma (CTCL). *Blood* 2007;**109**(1):31–9.
10. Munster P, Marchion D, Bicaku E, et al. Phase I trial of histone deacetylase inhibition by valproic acid followed by the topoisomerase II inhibitor epirubicin in advanced solid tumours: a clinical and translational study. *J Clin Oncol* 2007;**25**(15):1979–85.
11. Wang S, Yan-Neale Y, Cai R, Alimov I, Cohen D. Activation of mitochondrial pathway is crucial for tumour selective induction of apoptosis by LAQ824. *Cell Cycle* 2006;**5**(15):1662–8.
12. Takada Y, Gillenwater A, Ichikawa H, Aggarwal BB. Suberoylanilide hydroxamic acid potentiates apoptosis, inhibits invasion, and abolishes osteoclastogenesis by suppressing nuclear factor-kappaB activation. *J Biol Chem* 2006;**281**(9):5612–22.
13. Ungerstedt JS, Sowa Y, Xu WS, et al. Role of thioredoxin in the response of normal and transformed cells to histone deacetylase inhibitors. *Proc Natl Acad Sci USA* 2005;**102**(3):673–8.
14. Peart MJ, Tainton KM, Ruefli AA, et al. Novel mechanisms of apoptosis induced by histone deacetylase inhibitors. *Cancer Res* 2003;**63**(15):4460–71.
15. Zhu P, Huber E, Kiefer F, Gottlicher M. Specific and redundant functions of histone deacetylases in regulation of cell cycle and apoptosis. *Cell cycle* 2004;**3**(10):1240–2.
16. Del Duca D, Werbowetski T, Del Maestro RF. Spheroid preparation from hanging drops: characterization of a model of brain tumour invasion. *J Neurooncol* 2004;**67**(3):295–303.
17. Truchet I, Jozan S, Baron S, et al. Estrogen and antiestrogen-dependent regulation of breast cancer cell proliferation in multicellular spheroids: influence of cell microenvironment. *Int J Oncol* 2008;**32**(5):1033–9.
18. Sauer H, Klimm B, Hescheler J, Wartenberg M. Activation of p90RSK and growth stimulation of multicellular tumour spheroids are dependent on reactive oxygen species generated after purinergic receptor stimulation by ATP. *Faseb J* 2001;**15**(13):2539–41.
19. Wartenberg M, Hescheler J, Sauer H. Electrical fields enhance growth of cancer spheroids by reactive oxygen species and intracellular Ca^{2+}. *Am J Physiol* 1997;**272**(5 Pt 2): R1677–83.
20. Richon VM, Sandhoff TW, Rifkind RA, Marks PA. Histone deacetylase inhibitor selectively induces p21WAF1 expression and gene-associated histone acetylation. *Proc Natl Acad Sci USA* 2000;**97**(18):10014–9.
21. Altieri DC. The case for survivin as a regulator of microtubule dynamics and cell-death decisions. *Curr Opin Cell Biol* 2006;**18**(6):609–15.
22. Noh EJ, Lim DS, Jeong G, Lee JS. An HDAC inhibitor, trichostatin A, induces a delay at G2/M transition, slippage of spindle checkpoint, and cell death in a transcription-dependent manner. *Biochem Biophys Res Commun* 2009;**378**(3):326–31.
23. Grabowski P, Kuhnel T, Muhr-Wilkenshoff F, et al. Prognostic value of nuclear survivin expression in oesophageal squamous cell carcinoma. *Br J Cancer* 2003;**88**(1):115–9.
24. Ruefli AA, Ausserlechner MJ, Bernhard D, et al. The histone deacetylase inhibitor and chemotherapeutic agent suberoylanilide hydroxamic acid (SAHA) induces a cell-death pathway characterized by cleavage of Bid and production of reactive oxygen species. *Proc Natl Acad Sci USA* 2001;**98**(19):10833–8.
25. Arts J, Angibaud P, Marien A, et al. R306465 is a novel potent inhibitor of class I histone deacetylases with broad-spectrum antitumoural activity against solid and haematological malignancies. *Br J Cancer* 2007;**97**(10):1344–53.
26. Xu WS, Perez G, Ngo L, Gui CY, Marks PA. Induction of polyploidy by histone deacetylase inhibitor: a pathway for antitumour effects. *Cancer Res* 2005;**65**(17):7832–9.
27. Shin HJ, Baek KH, Jeon AH, et al. Inhibition of histone deacetylase activity increases chromosomal instability by the aberrant regulation of mitotic checkpoint activation. *Oncogene* 2003;**22**(25):3853–8.
28. Warrener R, Beamish H, Burgess A, et al. Tumour cell-selective cytotoxicity by targeting cell cycle checkpoints. *Faseb J* 2003;**17**(11):1550–2.
29. Taddei A, Maison C, Roche D, Almouzni G. Reversible disruption of pericentric heterochromatin and centromere function by inhibiting deacetylases. *Nat Cell Biol* 2001;**3**(2): 114–20.
30. Rosato RR, Almenara JA, Grant S. The histone deacetylase inhibitor MS-275 promotes differentiation or apoptosis in human leukemia cells through a process regulated by generation of reactive oxygen species and induction of p21CIP1/WAF1 1. *Cancer Res* 2003;**63**(13): 3637–45.
31. Burgess A, Ruefli A, Beamish H, et al. Histone deacetylase inhibitors specifically kill nonproliferating tumour cells. *Oncogene* 2004;**23**(40):6693–701.
32. Burgess AJ, Pavey S, Warrener R, et al. Up-regulation of p21(WAF1/CIP1) by histone deacetylase inhibitors reduces their cytotoxicity. *Mol Pharmacol* 2001;**60**(4):828–37.
33. Tupper J, Greco O, Tozer GM, Dachs GU. Analysis of the horseradish peroxidase/indole-3-acetic acid combination in a three-dimensional tumour model. *Cancer Gene Ther* 2004;**11**(7):508–13.
34. Nguyen DM, Schrump WD, Chen GA, et al. Abrogation of p21 expression by flavopiridol enhances depsipeptide-mediated apoptosis in malignant pleural mesothelioma cells. *Clin Cancer Res* 2004;**10**(5):1813–25.